Research Square

Preprints are preliminary reports that have not undergone peer review.
They should not be considered conclusive, used to inform clinical practice,
or referenced by the media as validated information.

Multi-omics analysis identifies BICC1+ fibroblasts drive triple negative breast cancer aggressiveness and poor prognosis

Shiyuan Zhang
Harbin Medical University Cancer Hospital
Hongnan Lu
Harbin Medical University Cancer Hospital
Yiwei Shen
Harbin Medical University Cancer Hospital
Yuan Yu
Harbin Medical University Cancer Hospital
Boqian Yu
Harbin Medical University Cancer Hospital
Chunlei Tan
Harbin Medical University Cancer Hospital
Shuqiang Liu
Harbin Medical University Cancer Hospital
Kun Qiao
Harbin Medical University Cancer Hospital
Xiangshi Lu
Harbin Medical University Cancer Hospital
Yuanxi Huang
rxwk@163.com

Harbin Medical University Cancer Hospital

Research Article

Keywords:

Posted Date: June 19th, 2026

DOI: https://doi.org/10.21203/rs.3.rs-9487369/v1

License: This work is licensed under a Creative Commons Attribution 4.0 International License.
Read Full License

Additional Declarations: No competing interests reported.

Abstract

Background

Triple negative breast cancer (TNBC) is an aggressive subtype with poor prognosis. Cancer-associated fibroblasts (CAFs) in the tumor microenvironment (TME) promote immunosuppression and drug resistance. This study identifies a specific fibroblast subpopulation driving TNBC progression.

Methods

We performed bulk, spatial transcriptomics (ST), single cell RNA sequencing (scRNA-seq), immunofluorescence staining of 80 TNBC samples, and functional assays including co-culture, proliferation, migration, and invasion experiments.

Results

BICC1 + fibroblasts correlated with resistance to immunotherapy and chemotherapy, and served as an independent prognostic factor for poor survival. These cells promoted TNBC cell invasiveness and drove M2 macrophage polarization via the ANGPTL4/SDC3 signaling axis, as revealed by scRNA-seq and ST.

Conclusions

BICC1 identifies a pathogenic CAFs subpopulation in TNBC that enhances tumor invasion and M2 macrophage polarization through ANGPTL4/SDC3 signaling, contributing to therapeutic resistance and an immunosuppressive microenvironment.

Introduction

Breast cancer has become the most common malignant tumor in women worldwide, and its incidence rate is continuing to rise and representing an escalating global health burden.[1] Triple negative breast cancer(TNBC) accounts for approximately 15% of all breast cancers and is considered a distinct molecular subtype.[2] TNBC is classically defined as a breast cancer subtype that lacks estrogen receptor (ER), progesterone receptor (PR), and human epidermal growth factor receptor-2 (HER-2) expression. Based on molecular features, it also can be further divided into four subtypes: immunomodulatory, luminal androgen receptor, basal-like immunosuppressive and mesenchymal.[3] The immunomodulatory subtype tends to have a better prognosis and more sensitive response to immunotherapy, providing a rationale for precision therapy approaches in TNBC. Recent advances in immune checkpoint inhibitors (ICIs) development have demonstrated significant therapeutic potential for TNBC patients, it has been discovered that ICIs demonstrate significant potential in the treatment of TNBC patients and are expected to become a new therapeutic target for TNBC. [4]

Cancer associated fibroblasts (CAFs) play a pivotal role in orchestrating the immunosuppressive landscape of the tumor microenvironment (TME) via multiple distinct mechanisms. From a metabolic

perspective, palmitic acid derived from tumor cells can activate CAFs, which in turn induces glutamine synthesis. This metabolic reprogramming of CAFs further facilitates the polarization of tumor associated macrophages (TAMs) toward the M2 phenotype.[5] Furthermore, tryptophan 2,3-dioxygenase-positive matrix fibroblasts (TDO2+ MFs) within lung metastatic lesions secrete kynurenine, a metabolite that not only confers disseminated tumor cells resistance to ferroptosis but also impairs T cell function, ultimately contributing to the progression of lung metastasis in breast cancer.[6] From an immunological perspective, CAFs are capable of acting as "sacrificial decoys". Specifically, direct interaction between CAFs and natural killer (NK) cells results in the lysis of CAFs, which in turn induces the downregulation of activating receptors on NK cells and thereby confers protection to cancer cells.[7,8] In addition to their role in immune modulation, CAFs facilitate malignant progression via direct paracrine pathways. Specifically, exosomal circular RNA circMIB1 is able to be translated into the functional peptide MIB1-223aa, which enhances the stability of MIB1 protein to activate Notch signaling. This process further promotes metastasis and cancer stemness in TNBC.[9] Similarly, there exists a unique senescent-like TSPAN8+ myofibroblast subpopulation, the formation of which is associated with the degradation of SIRT6 protein. This specific subpopulation contributes to the enhancement of cancer cell stemness and chemoresistance by secreting IL-6 and IL-8.[10] Furthermore, sphingosine kinase 2 (SphK2) derived from matrix fibroblasts contributes to the establishment of a pro-tumorigenic microenvironment. Specifically, this kinase inhibits p53 activity and drives the transformation of fibroblasts into phenotypes that promote tumor progression.[11] Despite these progresses, the specific fibroblast subpopulations resident in the TNBC microenvironment, as well as their elaborate regulatory mechanisms underlying the molding of TME dynamics and immunotherapy responsiveness remain to be fully elucidated.

Bicistronic intergenic C-homologous protein 1 (BICC1) belongs to the family of RNA-binding proteins, which exerts post-transcriptional regulatory effects on a variety of cytoplasmic mRNAs. In terms of structure, BICC1 is characterized by tandem N-terminal K-homology and KH-like domains, alongside serine-glycine-rich sequences and a sterile α-motif (SAM) domain at its C-terminus.[12] Functionally, BICC1 has been identified as a key oncogenic regulator in pancreatic ductal adenocarcinoma (PDAC). And it not only promotes cancer stemness but also induces resistance to gemcitabine. Importantly, targeted suppression of BICC1 signaling has been shown to substantially improve the efficacy of chemotherapy.[13] In addition, increased BICC1 expression in gastric cancer is associated with poor clinical prognosis and higher infiltration of immunosuppressive cells, including M2 macrophages and regulatory T cells, which imply that BICC1 may accelerate tumor progression by modulating the TME.[14] Despite the considerable advances of BICC1 made in other cancer types, its prognostic value in TNBC and the specific mechanisms through which it regulates the TME have not yet been investigated.

Multi-omics strategies were employed to identify key fibroblast subpopulations in TNBC and clarify their influences on the TME and clinical prognosis in our study. We found that BICC1 is mainly expressed in fibroblasts within the TNBC microenvironment through single cell RNA transcriptomic sequencing (scRNA-seq) analysis and immune infiltration profiling. Of note, both increased BICC1 expression and higher abundance of BICC1+ fibroblasts were correlated with poor immunotherapy response and

unfavorable survival outcomes, such as reduced disease free survival (DFS) and overall survival (OS). In vitro co-culture assays showed that knockdown of BICC1 in fibroblasts markedly weakened the invasive ability of TNBC cell lines. Moreover, cell-cell communication analysis and spatial transcriptomics (ST) assays revealed a close spatial association between BICC1+ fibroblasts and SDC3+ macrophages in TNBC tissues. These results indicate that BICC1+ fibroblasts may induce M2 polarization of SDC3+ macrophages via ANGPTL4-mediated signaling pathways, which contribute to adverse clinical outcomes and immunotherapy resistance in TNBC. Collectively, our study clarifies the role of BICC1+ fibroblasts in regulating the TNBC immune microenvironment, which improves our understanding of survival differences and heterogeneous immunotherapy responses in patients with TNBC. The research design is shown in the flowchart (Figure 1).

Methods

Bulk transcriptome sequencing data analysis

Transcriptomic profiles and clinical data were analyzed from a variety of public data repositories in this study. Specifically, bulk RNA-seq data and corresponding clinical annotations for The Cancer Genome Atlas Breast Invasive Carcinoma (TCGA-BRCA) cohort were acquired from the UCSC Xena browser (https://xenabrowser.net/datapages/), whereas data derived from the Molecular Taxonomy of Breast Cancer International Consortium (METABRIC) were retrieved from cBioPortal (https://www.cbioportal.org/). There were 159 TNBC cases from TCGA and 298 TNBC cases from METABRIC were selected in these two cohorts. These cases met the criteria of estrogen receptor (ER), progesterone receptor (PR), and human epidermal growth factor receptor 2 (HER-2) negatively expression or were classified as basal subtype based on the PAM50 classification system. Furthermore, bulk RNA-seq datasets were downloaded from the Gene Expression Omnibus (GEO) database, including datasets from TNBC patients who received neoadjuvant chemotherapy (paclitaxel or anthracycline-based regimens; GSE20271) and those treated with neoadjuvant immunotherapy in combination with chemotherapy (GSE196096). Differentially expressed genes (DEGs) between patients achieving pathological complete response (pCR) and non-pathological complete response (non-pCR) were identified using the DESeq2 package in R. BICC1 expression levels were also compared between TNBC and adjacent normal breast tissues in the TCGA-BRCA cohort. Prognostic associations of BICC1 and ANGPTL4 with OS and distant metastasis free survival (DMFS) in breast cancer who were classified as basal subtype were evaluated on the Kaplan-Meier Plotter website (https://kmplot.com/analysis/).[15] Fibroblast proportions in GSE196096 and GSE20271 samples were deconvoluted using the EPIC platform (https://epic.gfellerlab.org/). Samples were stratified by median BICC1 expression and fibroblast infiltration levels. The high BICC1+ fibroblast group comprised samples with above median values for both parameters, while the low BICC1+ fibroblast group included samples with below median values for both. Immune infiltration patterns in TCGA and METABRIC TNBC samples were assessed using EPIC, CIBERSORT and Xcell algorithms, respectively.

scRNA-seq analysis

The scRNA-seq data from nine TNBC samples (GSE176078) were downloaded from the GEO database. Analysis was performed using the Seurat package in R. Cells with more than 25% mitochondrial gene expression or fewer than 200 detected genes, as appropriate, were removed during quality control filtering. Logarithmic normalization was applied, followed by identification of 2,000 highly variable genes (HVGs) and batch effect correction using Harmony package. Dimensionality reduction was conducted using principal component analysis (PCA), with uniform manifold approximation and projection (UMAP) employed for visualization. Annotation of cell types and subtypes was based on established marker genes.[16] DEGs were identified using the FindAllMarkers function (from Seurat package) with thresholds of $|\log_2(\text{fold change})| > 1$ (or 0.5) and adjusted p-value < 0.05. Cell-cell communication analysis was conducted using the CellChat package, which queries the CellPhoneDB database to infer ligand-receptor interactions between cell populations. Interaction strengths were visualized using netVisual_bubble and netVisual_circle functions.

ST data analysis

ST data from TNBC specimens were obtained from the Zenodo repository (Andersson et al. https://zenodo.org/record/3957257)[17] and the GEO database (GSE210616).[18] Data processing and visualization were performed in R using the Seurat package. Tissue spots with zero or minimal unique molecular identifier (UMI) counts were removed during quality control. Dimensionality reduction was achieved with PCA and UMAP following batch correction with harmony package, and clusters were identified using graph-based methods. Cell type deconvolution was carried out using SPOTlight, which integrates scRNA-seq derived marker genes with ST data to estimate the composition of cell subpopulations. Results were visualized on tissue sections, and subpopulation abundance scores were computed. Spatial associations between cell types were assessed using Pearson correlation. Cell-cell communication networks were inferred from the spatial transcriptomics data using the CellChat package, with interaction strengths visualized via netVisual_heatmap and netVisual_aggregate functions.

Functional enrichment analysis

To elucidate the biological functions of BICC1 in TNBC, we performed stratified enrichment analyses using 159 TCGA-BRCA cases grouped by BICC1 expression levels. We annotated fibroblast subtypes in nine TNBC samples from scRNA-seq dataset GSE176078 and conducted gene set enrichment analysis (GSEA) comparing BICC1+ versus BICC1- fibroblasts. All enrichment analyses were carried out with the clusterProfiler package in R, encompassing Gene Ontology (GO) biological process enrichment, Kyoto Encyclopedia of Genes and Genomes (KEGG) pathway analysis, and Hallmark gene sets from MSigDB. Statistical significance was defined by an FDR threshold of less than 0.05.

Immunofluorescence Assay

Eighty TNBC cases were retrospectively collected from the institutional database of Harbin Medical University Cancer Hospital. All cases were confirmed as ER-negative and PR-negative by

immunohistochemistry, with HER-2 immunohistochemistry scores of 0 or 1. Cases with HER-2 IHC score 2+ underwent confirmatory fluorescence in situ hybridization (FISH) testing to rule out HER-2 amplification. Histopathological diagnosis was independently reviewed by two certified pathologists. Tissue sections were subjected to dual immunofluorescence staining using anti-BICC1 antibody (Cat. CSB-PA872503LA01HU, Cusabio) and anti-α-SMA antibody (Cat. ab7817, Abcam). Whole-slide images were captured and examined using CaseViewer. Quantification of BICC1+ α-SMA+ fibroblasts was performed by averaging the counts from three randomly selected high-power fields (40× objective) per sample. Patients were stratified into high or low BICC1+ α-SMA+ fibroblast infiltration groups using the median cell count as the cutoff.

Cell Lines

The human TNBC cell line MDA-MB-231 was purchased from AOYINBIO (Cat. SAc0237). Cells were cultured in complete growth medium supplemented with 10% fetal bovine serum (FBS; Cell-box, Cat. AUS-01S-02), 100 U/mL penicillin, and 100 μg/mL streptomycin (Cell-Box, Cat. CBKSS-M0008) at 37°C with 5% CO_2 in a humidified incubator.

Primary fibroblast isolation from tumor samples

Primary TNBC samples were obtained from patients who underwent therapeutic surgery at Harbin Medical University Cancer Hospital (Ethics Approval Number: KY2026-10). Fresh tumor tissues and adjacent normal tissues (controls) were collected under sterile conditions and transported in ice-cold DMEM/F12 (Gibco, Cat. C11995500BT) medium containing high-concentration penicillin-streptomycin (2-5×). Tissues were washed with ice-cold phosphate buffered saline (PBS, Share-Bio, Cat. SB-CR017, 1% penicillin-streptomycin), minced into 1-2 mm^3 fragments after removing adipose tissue, necrotic regions, and fibrous capsules. Tissue fragments were evenly distributed in culture flasks, inverted, and incubated at 37°C with 5% CO_2 for 2-4 hours to allow adhesion. After returning flasks to an upright orientation, cultures were maintained in complete medium with half-volume changes every 2–3 days. Fibroblast outgrowth was detected within 5–14 days. Upon reaching 70–80% confluence, cells were dissociated using 0.25% trypsin-EDTA (Gibco, 1–3 minutes) and subjected to differential adhesion for 20–30 minutes, allowing selective attachment of fibroblasts while contaminating cells remained in suspension. This purification procedure was repeated at each passage to preserve fibroblast purity throughout the culture period.

Quantitative real-time PCR

Total RNA was isolated from fibroblasts using TRIzol (Invitrogen), reverse-transcribed using the Roche RT Kit, and subjected to quantitative real-time PCR (qRT-PCR) with SYBR Green (Roche). Gene expression was normalized to GAPDH. Primer sequences: ***ANGPTL4 (F: 5′-CTCAAGGCTCAGAACAGCAGG-3′, R: 5′-TGGTCCAGGAGGCCAAACT-3′); BICC1 (F: 5′-TCCAGGGCACCATTGAGT-3′, R: 5′-CTTGGCTGTTTGGGCTTT-3′).***

Transfection and co-culture

MDA-MB-231 cells were cultured in high-glucose DMEM containing 10% FBS and 1% penicillin-streptomycin at 37°C with 5% CO_2. BICC1 expression in CAFs was silenced using BICC1-specific siRNA (Genepharma) delivered via Lipofectamine 2000 (Invitrogen, Carlsbad, CA) following the manufacturer's instructions. The BICC1-specific siRNA sense sequence was ***5′-GGAAGAAACUUGAGGCCAUTTAUGGCCUCAAGUUUCUUCCTT-3′***.CAFs were harvested 48 hours post-transfection using trypsin-EDTA, washed with PBS, and plated in the upper chambers of Transwell® inserts (0.4 μm pores; Corning) at a ratio of 1:5 relative to MDA-MB-231 cells. After 48 hours of co-culture, MDA-MB-231 cells were collected for subsequent functional analyses.

Cell proliferation assay

Cell proliferation was assessed using the Cell Counting Kit-8 (CCK-8; Share-Bio, Cat. SB-CCK8) according to the manufacturer's protocol. At specified time points (0, 24, 48, 72, and 96 hours), 10 μL of CCK-8 reagent was added to each well. After 2 hours of incubation at 37°C, absorbance at 450 nm was measured with a microplate reader. Proliferation was quantified relative to the control and normalized to the initial measurement. All data are shown as mean ± standard deviation (SD) from three independent experiments.

Invasion and Migration assay

Transwell assays (8μm pores; Corning) were employed to evaluate cell migration and invasion. For invasion assays, the upper chamber membranes were coated with extracellular matrix gel diluted in serum-free medium, while migration assays utilized uncoated membranes. Serum-starved cells (5×10^4 per well) were suspended in serum-free medium and placed in the upper chambers, with 10% FBS medium in the lower chambers serving as a chemoattractant. Following 40 hours of incubation at 37°C, non-migrated or non-invaded cells were removed from the upper membrane surface. Cells that traversed the membrane were fixed in 4% paraformaldehyde, stained with 0.1% crystal violet, and observed under an inverted microscope. Cell counts from at least three randomly selected fields per insert were used for quantification via ImageJ software.

Wound healing

Cell migration was analyzed using the scratch (wound healing) assay. Monolayers were grown to >90% confluence, after which a sterile pipette tip was employed to create a uniform linear scratch. Detached cells and debris were removed with PBS, and low-serum medium (1–2% FBS) was applied to minimize proliferation. Phase-contrast images were obtained immediately (0 hours) and 48 hours after scratching using an inverted microscope. Cells were incubated at 37°C with 5% CO_2 throughout. The extent of wound closure was determined with ImageJ using the formula: [(initial wound area − remaining wound area at 48 h) / initial wound area] × 100%.

Statistical analysis

Continuous measurements are reported as mean ± standard deviation (SD) and were analyzed using Student's t-test or one-way ANOVA, as appropriate. Categorical variables are presented as n (%) and analyzed with χ^2 or Fisher's exact test. Survival outcomes were evaluated using Kaplan–Meier estimates and compared with the log-rank test. Multivariate survival analyses were performed using Cox proportional hazards regression with stepwise selection of covariates. Pearson correlation coefficients were calculated to examine linear associations. All statistical analyses were performed using GraphPad Prism 8.0 and R (version 4.4.2), with two-sided p-values < 0.05 considered statistically significant.

Results

Annotation of fibroblast subtypes in TNBC

Single-cell transcriptomic analysis of TNBC samples from the GSE176078 dataset revealed eight major cell lineages: T cells, B cells, plasma cells, myeloid cells, epithelial cells, endothelial cells, mesenchymal cells, and proliferating cells (Fig. 2A). The relative abundance of these populations varied substantially between patients (Fig. 2B). Canonical marker genes confirmed cell type identities, including CD3D (T cells), MS4A1 (B cells), CD68 (myeloid cells), PDGFRB (mesenchymal cells), MKI67 (proliferating cells), EPCAM (epithelial cells), JCHAIN (plasma cells), and PECAM1 (endothelial cells) (Fig. 2C). Further subclustering of mesenchymal cells distinguished three subsets: CAFs, endothelial cells, and perivascular-like (PVL) cells (Fig. 2D). Marker gene analysis demonstrated that CAFs were characterized by ACTA2, MCAM, and COL1A1, endothelial cells by PECAM1 and CD34, and PVL cells by PDGFRB and PDGFRA (Fig. 2E). These refined classifications enabled updated profiling of cellular composition across all TNBC samples (Fig. 2F, G), establishing a robust framework for investigating fibroblast heterogeneity.

Multi-omics analyses reveal a BICC1 + fibroblast subpopulation linked to immunotherapy response in TNBC.

To investigate fibroblast markers linked to immunotherapy response in TNBC, the GSE196096 dataset comprising 29 patients treated with neoadjuvant chemotherapy and pembrolizumab was analyzed. Differential expression analysis between non-pCR and pCR groups intersected with established fibroblast markers identified seven candidate genes (Fig. 3A), with BICC1 notably upregulated in non-pCR patients (Fig. 3B). UMAP visualization confirmed that BICC1 expression was restricted to the CAF subpopulation (Fig. 3C) and significantly higher in CAFs compared to other cell types (Fig. 3D). Validation in independent TNBC cohorts (GSE196096 and GSE20271) consistently demonstrated elevated BICC1 levels in non-pCR versus pCR patients (Fig. 3E, F), and high BICC1 + fibroblast infiltration was associated with non-pCR status (Fig. 3G, H). Survival analyses indicated that elevated BICC1 expression predicted worse DMFS and OS (Fig. 3I, J). Analysis of TCGA-BRCA data revealed lower BICC1 expression in TNBC tissues relative to normal breast tissue (Fig. 3K), reflecting its stromal localization. Collectively, these findings highlight the BICC1 + fibroblast subpopulation as a potential predictive biomarker for immunotherapy response and clinical outcomes in TNBC.

Immune infiltration analysis of BICC1 in TNBC patients

We examined correlations between BICC1 levels and fibroblast abundance in the TCGA-TNBC and METABRIC-TNBC cohorts using the Xcell and EPIC deconvolution algorithms to investigate the relationship between BICC1 expression and the TME. BICC1 expression showed significant positive correlations with fibroblast scores in both cohorts (TCGA-TNBC: Pearson r = 0.50, P = 3.00×10^{-11}; METABRIC-TNBC: Pearson r = 0.33, P = 5.45×10^{-9} [Xcell]) (Fig. 4A, B). Similarly, BICC1 levels correlated positively with CAFs proportions (TCGA-TNBC: Pearson r = 0.42, P = 2.72×10^{-8}; METABRIC-TNBC: Pearson r = 0.43, P = 7.78×10^{-15} [EPIC]) (Fig. 4C, D). Furthermore, analysis revealed that StromaScore and MicroenvironmentScore were markedly elevated in TNBC samples with high BICC1 expression relative to those with low expression (Fig. 4E, F). These results indicate that high BICC1 expression is closely linked to tumor stromal accumulation and an immunosuppressive microenvironment.

Functional characterization of BICC1 through enrichment analysis

Differential expression analysis was performed on the TCGA-TNBC dataset to explore the biological functions of BICC1 by comparing samples with high versus low BICC1 expression. GO enrichment analysis revealed that upregulated genes were significantly enriched in biological processes related to extracellular matrix (ECM) organization, cell-cell adhesion, hormone metabolism. Cellular components were associated with collagen-containing ECM, endoplasmic reticulum lumen, and Golgi apparatus. And molecular functions involved in ECM structural constituents, glycosaminoglycan binding, and serine-type endopeptidase activity (Fig. 5A). KEGG pathway analysis further identified enrichment in neuroactive ligand-receptor interactions, ECM-receptor interactions, protein digestion and absorption, and PI3K-Akt signaling pathways (Fig. 5B). A Circos plot illustrated the integrated network between key genes and these pathways (Fig. 5C). To investigate cell-type-specific functions, we stratified CAFs from the GSE176078 scRNA-seq dataset into BICC1 + and BICC1- subpopulations based on BICC1 expression. Differential gene analysis followed by GO enrichment revealed that BICC1 + CAFs exhibited upregulation of genes involved in cell adhesion, immune response regulation, and protein metabolism (Fig. 5D). GSEA further indicated that BICC1 + CAFs negatively regulate immune response, immune system processes, and programmed cell death pathways (Fig S1a–d). Collectively, these functional characteristics suggest that BICC1 + fibroblasts may promote TNBC progression through extracellular matrix remodeling and immunomodulation.

A higher abundance of BICC1 + fibroblasts is associated with worse clinical outcomes in TNBC

Dual-label immunofluorescence staining was performed on tissue sections from 80 TNBC patients to validate the clinical significance of BICC1 + fibroblasts. This analysis confirmed co-expression of BICC1 with the fibroblast-specific marker α-SMA in TNBC tissues (Fig. 6A, B). Based on quantitative immunofluorescence scoring, patients were stratified into high BICC1 + fibroblast infiltration and low

infiltration groups (n = 40 per group). Kaplan–Meier survival analysis demonstrated significantly inferior DFS and OS in the high infiltration group compared with the low infiltration group (Fig. 6C, D; both $P \leq 0.001$). Analysis of baseline clinicopathological characteristics revealed no significant between-group differences in age, T stage, histological grade, Ki67 proliferation index, or tumor-infiltrating lymphocytes (TILs) density. However, the high infiltration group exhibited more advanced nodal stage (N2–3: 37.5% vs. 7.5%, P = 0.008) and higher rates of lymphovascular invasion (37.5% vs. 12.5%, P = 0.020) (Table 1). Univariate and multivariate Cox proportional hazards regression analyses identified high BICC1 + fibroblast infiltration as an independent adverse prognostic factor for both DFS (hazard ratio [HR] = 2.44, 95% confidence interval [CI]: 1.19–5.03, P = 0.015) and OS (HR = 2.28, 95% CI: 1.03–5.05, P = 0.043) (Fig. 6E, F). These findings establish BICC1 + fibroblast infiltration as a robust prognostic indicator in TNBC.

Table 1
Baseline Characteristics

n	Overall	High BICC1 + Fibroblast	Low BICC1 + Fibroblast	P
	80	**40**	**40**	
Age(%)				0.494
≤ 50	32(40.0)	18(45.0)	14(35.0)	
>50	48(60.0)	22(55.0)	26(65.0)	
T(%)				0.363
1	52 (65.0)	23 (57.5)	29 (72.5)	
2	25 (31.2)	15 (37.5)	10 (25.0)	
3	3 (3.8)	2 (5.0)	1 (2.5)	
N(%)				**0.008**
0	49 (61.3)	20 (50.0)	29 (72.5)	
1	13 (16.2)	5 (12.5)	8 (20.0)	
2	10 (12.5)	7 (17.5)	3 (7.5)	
3	8 (10.0)	8 (20.0)	0 (0.0)	
G(%)				0.567
2	15(18.8)	6(15.0)	9(22.5)	
3	65(81.2)	34(85.0)	31(77.5)	
KI67(%)				0.453
≤ 30%	22(27.5)	9(22.5)	13(32.5)	
>30%	58(72.5)	31(77.5)	27(67.5)	
TILs(%)#				0.823
<10%	40(50.0)	21(52.5)	19(47.5)	
≥ 10%	40(50.0)	19(47.5)	21(52.5)	
LVI(%)*				**0.020**
negative	60(75.0)	25(62.5)	35(87.5)	
# Tumor-Infiltrating Lymphocytes				
* Lymphovascular Invasion				

n	Overall	High BICC1 + Fibroblast	Low BICC1 + Fibroblast	P
	80	**40**	**40**	
positive	20(25.0)	15(37.5)	5(12.5)	
# Tumor-Infiltrating Lymphocytes				
* Lymphovascular Invasion				

BICC1 + fibroblasts may interact with macrophages via the ANGPTL4/SDC3 signaling pathway in TNBC
We reclustered CAFs into BICC1 + and BICC1- subpopulations to investigate interactions between BICC1 + fibroblasts and other cellular compartments within the TME (Fig. 7A). CellChat analysis revealed extensive ligand–receptor interactions between BICC1 + CAFs and multiple immune cell types, with myeloid cells showing particularly robust communication (Fig. 7B). Specifically, BICC1 + CAFs engaged myeloid cells through several ligand–receptor pairs, including ANGPTL4–SDC3, JAM2–(ITGAV+ITGB1), and ANGPTL2–PIRB (Fig. 7C). UMAP visualization confirmed specific expression of ANGPTL4–SDC3 (Fig. 7D–G) and ANGPTL2–PIRB (Fig S2a–d) in BICC1 + CAFs and myeloid cells, respectively, whereas JAM2–(ITGAV+ITGB1) showed no specific enrichment in these populations (Fig. S2e–j). Analysis of patient survival indicated a significant association between high ANGPTL4 expression and unfavorable outcomes in TNBC (Fig. 7H, I), whereas ANGPTL1 showed no significant prognostic association (Fig S2k, l). Network analysis visualized the communication intensity between BICC1 + CAFs and myeloid cells specifically via the ANGPTL signaling axis (Fig. 7J). These findings indicate that BICC1 + fibroblasts may regulate the TME through the ANGPTL4-SDC3 signaling axis. To validate this mechanism, immune cell infiltration was analyzed using CIBERSORT in TCGA-TNBC (Fig. 8A, B) and METABRIC-TNBC (Fig. 8C, D) datasets. ANGPTL4 expression was inversely correlated with M1 macrophage levels and positively correlated with M2 macrophage infiltration, supporting a potential role of the ANGPTL4-SDC3 axis in promoting M2 polarization within the TME.

ST identifies the spatial proximity of BICC1⁺ fibroblasts and SDC3⁺ macrophages within TNBC tissue

We analyzed spatial transcriptomics data from TNBC samples to validate the spatial colocalization of BICC1 + fibroblasts and SDC3 + macrophages at the tissue level. Quality control assessment identified two samples (GSM6433585 and CID44971) with adequate sequencing depth and spatial resolution (Fig. 9A, D). Spatial mapping revealed distinct colocalization patterns between BICC1 + CAFs and SDC3 + macrophages within tumor tissues (Fig. 9B, C, E, F). Correlation analysis demonstrated a significant positive association between the proportions of these cell populations (Pearson R = 0.37, P = 1.38×10^{-42}) (Fig. 9G). CellChat analysis of spatial cell-cell communication further validated active ANGPTL signaling between BICC1 + CAFs and SDC3 + macrophages (Fig. 9H, I). Interaction network heatmaps indicated that BICC1 + CAFs function as the predominant signal senders, whereas SDC3 + macrophages

serve as the primary recipients (Fig. 9J, K). Collectively, these spatial transcriptomic data provide in situ evidence that BICC1 + fibroblasts interact with macrophages via the ANGPTL4–SDC3 axis.
To determine the functional impact of BICC1 + fibroblasts on TNBC cell behavior, we performed RNA interference-mediated knockdown of BICC1 in CAFs. Validation of transfection efficiency demonstrated ~ 85% reduction in BICC1 mRNA levels, with concomitant downregulation of its downstream effector ANGPTL4 (Fig. 10A). In vitro functional assays revealed that TNBC cells exposed to conditioned medium from BICC1-knockdown CAFs exhibited significantly reduced proliferation compared with cells treated with control medium (Fig. 10B). Both Transwell migration and invasion assays showed a notable decrease in cell motility and invasiveness under knockdown conditions (Fig. 10C, D). Consistent results were observed in wound healing assays, where BICC1-deficient CAF-conditioned medium substantially attenuated TNBC cell migratory capacity (Fig. 10E). These experiments collectively demonstrate that BICC1 + fibroblasts drive TNBC cell proliferation, invasion, and migration via paracrine signaling, thereby promoting malignant behavior.

Discussion

TNBC is an aggressive subtype lacking expression of ER, PR, and HER2, resulting in restricted treatment options and inferior clinical outcomes compared with other breast cancer types.[19] TME has been identified as a major determinant of TNBC progression and therapeutic resistance. CAFs constitute a major stromal component, playing key roles in tumor growth, immune suppression, and therapy resistance. CAFs are heterogeneous, originating from diverse sources and exhibiting phenotypic plasticity during tumor evolution. They are primarily categorized into myofibroblastic CAFs (myCAFs), inflammatory CAFs (iCAFs), and antigen-presenting CAFs (apCAFs) based on transcriptional and functional features.[20] In TNBC, myCAFs are particularly abundant, marked by α-SMA expression and robust ECM production and remodeling. Jagged1, a Notch ligand, has been shown to regulate CAF-driven ECM remodeling, with elevated Jagged1 expression in TNBC cells associated with poor prognosis and the promotion of myCAF polarization via TGFβ pathway activation, enhanced contractility, and upregulation of ECM-related genes.[21]

In addition to their role in ECM remodeling, CAFs serve as critical regulators of immune cell function within the tumor microenvironment. By engaging multiple immune cell types, CAFs establish an immunosuppressive environment that facilitates tumor immune evasion.[22] TAMs, a predominant immune component of the TME, often exhibit M2-like pro-tumorigenic polarization. Recent studies identified an AKAP12^{+} CAF subpopulation in TNBC associated with poor response to immunotherapy; mechanistically, these CAFs enhance IL-34 secretion via PI3K/AKT signaling, promoting M2 macrophage polarization through the IL-34/CSF1R pathway.[23] CAFs also contribute to T-cell dysfunction, a major mechanism of immune escape, with adipocyte enhancer-binding protein 1 (AEBP1)—highly expressed in CAFs and linked to unfavorable prognosis—driving T-cell impairment, as confirmed by scRNA-seq.[24] Given their multifaceted roles, CAFs-targeted strategies are being explored; however, early clinical trials using global CAFs depletion have produced limited efficacy and occasionally pro-tumorigenic effects,

underscoring the need for deeper insights into CAFs heterogeneity and function.[25]The RNA-binding protein BICC1 was initially discovered in Drosophila as a key regulator of embryonic development and has more recently been associated with cancer progression. Zhao et al. demonstrated that BICC1 serves as a prognostic biomarker in gastric cancer, with elevated expression correlating with immune infiltration.[14] Consistent with these findings, our study reveals that BICC1 is specifically and highly expressed in TNBC-associated CAFs, indicating that BICC1 + CAFs may constitute a conserved stromal subset that promotes tumor progression across cancer types.

This study elucidates the mechanistic role of BICC1 + CAFs in TNBC through the ANGPTL4–SDC3 signaling axis, highlighting their interaction with SDC3⁺ macrophages. ANGPTL4, a secreted glycoprotein, contributes to tumor progression via angiogenesis, metabolic reprogramming, and immune suppression.[26] Previous work has shown that CAF-derived ANGPTL4 regulates mitochondrial metabolism and decreases chemotherapy sensitivity.[27] Our study demonstrates that BICC1 + CAFs exhibit high ANGPTL4 expression and interact with SDC3⁺ macrophages through the ANGPTL4–SDC3 axis. These findings are consistent with prior reports by Fan et al., who showed that FGF19-activated hepatic stellate cells secrete ANGPTL4 to facilitate liver metastasis in colorectal cancer,[28] suggesting that ANGPTL4-mediated stromal-immune communication may be a broadly conserved mechanism in cancer. From a metabolic perspective, Ohri et al. reported persistent ANGPTL4 upregulation in pancreatic fibroblasts during early tumorigenesis, highlighting its role in promoting tumor progression via paracrine signaling loops.[29] Previous research by Zeng et al. demonstrated that CD36 + CAFs drive CD8 + T-cell exhaustion through the OxLDL–PPARγ–ANGPTL4 signaling pathway, contributing to immunotherapy resistance in osteosarcoma.[30] These studies corroborate our findings, indicating that ANGPTL4 functions as a critical molecular node connecting stromal metabolic reprogramming to the immunosuppressive tumor microenvironment. Additionally, Li et al. have characterized CAFs–tumor-associated macrophage interactions in lung adenocarcinoma through integrated bulk and single-cell RNA sequencing, providing further insight into stromal-immune crosstalk.[31] In the present study, we extend previous observations by characterizing the specific crosstalk between BICC1⁺ CAFs and SDC3⁺ macrophages via the ANGPTL4–SDC3 axis, validated at the tissue level through spatial transcriptomics to provide accurate spatial resolution of stromal-immune interactions. Previous meta-analyses have demonstrated that ANGPTL4 overexpression predicts poor survival in various malignancies.[32] In contrast, our findings establish BICC1 as a CAF-specific marker that is significantly associated with TNBC prognosis, independent of traditional clinicopathological factors, suggesting its utility as a novel molecular indicator for risk stratification.

SDC3 (Syndecan-3) has been implicated in TME regulation, with Habenicht et al. reporting its role as a heparan sulfate proteoglycan in breast cancer pathophysiology[33] and Lee et al. demonstrating its positive effect on macrophage pro-inflammatory function.[34] Our ST analyses verified that BICC1 + CAFs and SDC3 + macrophages are spatially co-localized, with CellChat analysis revealing active ANGPTL4–SDC3 signaling between these populations. These results support the hypothesis that BICC1 + CAFs drive M2 macrophage polarization through the ANGPTL4–SDC3 axis, thereby fostering an

immunosuppressive tumor microenvironment, consistent with analogous stromal-immune interactions described by Feng et al. in rhabdomyosarcoma.[35]

This study has several limitations. First, although bioinformatic analyses were combined with in vitro experiments, validation in larger, independent clinical cohorts is necessary. Second, the precise molecular mechanisms by which BICC1 regulates ANGPTL4 remain unclear. As an RNA-binding protein, BICC1 may affect ANGPTL4 mRNA stability or translation, but direct experimental evidence is lacking. Third, while we focused on interactions between BICC1 + CAFs and macrophages, CAFs also engage with other immune cells, including T cells and NK cells, as well as with tumor cells through multiple pathways, and the impact of these interactions on TNBC progression warrants further study. Finally, the absence of in vivo models limits the assessment of BICC1 + CAF function in tumor development and their potential as therapeutic targets. Future studies using genetically engineered or patient-derived xenograft models are planned to address this gap.

Conclusions

In conclusion, this study comprehensively characterizes the molecular features, clinical relevance, and regulatory mechanisms of BICC1 + CAFs in TNBC using integrated multi-omics analyses. We identify BICC1 as a CAF-specific marker in TNBC, with elevated expression associated with poor prognosis. Mechanistically, BICC1 + CAFs engage TAMs via the ANGPTL4–SDC3 signaling pathway, fostering an immunosuppressive tumor microenvironment. These findings provide a basis for the development of therapeutic strategies targeting stromal-immune interactions. Future work will aim to clarify how BICC1 regulates ANGPTL4 and evaluate the potential of BICC1 + CAF-targeted interventions in preclinical models.

Abbreviations

AEBP1	Adipocyte enhancer-binding protein 1
apCAF	Antigen-presenting cancer-associated fibroblast
BICC1	Bicistronic intergenic C-homologous protein 1
CAFs	Cancer-associated fibroblasts
CI	Confidence interval
CCK-8	Cell Counting Kit-8
DEGs	Differentially expressed genes
DFS	Disease free survival
DMFS	Distant metastasis free survival
ER	Estrogen receptor
FBS	Fetal bovine serum
FISH	Fluorescence in situ hybridization
GEO	Gene Expression Omnibus
GO	Gene Ontology
GSEA	Gene set enrichment analysis
HER-2	Human epidermal growth factor receptor-2
HR	Hazard ratio
HVGs	Highly variable genes
iCAF	Inflammatory cancer-associated fibroblast
ICIs	Immune checkpoint inhibitors
KEGG	Kyoto Encyclopedia of Genes and Genomes
METABRIC	Molecular Taxonomy of Breast Cancer International Consortium
myCAF	Myofibroblastic cancer-associated fibroblast
NK	Natural killer
non-pCR	non-pathological complete response
OS	Overall Survival
PBS	Phosphate buffered saline
PCA	Principal component analysis
pCR	pathological complete response

PDAC	**Pancreatic ductal adenocarcinoma**
PR	**Progesterone receptor**
PVL	**Perivascular-like**
qRT-PCR	**Quantitative real-time PCR**
SAM	**Sterile α-motif**
scRNA-seq	**single cell RNA sequencing**
SD	**Standard deviation**
SDC3	**Syndecan 3**
SphK2	**Sphingosine kinase 2**
ST	**Spatial transcriptomics**
TCGA-BRCA	**The Cancer Genome Atlas Breast Invasive Carcinoma**
TDO2+ MFs	**Tryptophan 2,3-dioxygenase-positive matrix fibroblasts**
TILs	**Tumor-infiltrating lymphocytes**
TME	**Tumor microenvironment**
TNBC	**Triple Negative Breast Cancer**
TAM	**Tumor Associated Macrophage**
UMAP	**Uniform manifold approximation and projection**
UMI	**Unique molecular identifier**

Declarations

Acknowledgments

We thank the patients who participated in this study and the clinical staff of Harbin Medical University Cancer Hospital for their assistance with sample collection.

Conflict of interest statement

The authors declare that they have no competing financial interests or personal relationships that could have influenced the work reported in this paper. No commercial entity provided financial support or materials for this study.

Availability of data and material

All data supporting the findings of this study are available within the paper. Single-cell transcriptomic data (GSE176078), bulk RNA-seq data (TCGA-BRCA, METABRIC), and spatial transcriptomics datasets analyzed during the current study are publicly available from the Gene Expression Omnibus (GEO), UCSC Xena Browser, and Zenodo repository (as cited in the Methods). Raw data supporting the findings are available from the corresponding author upon reasonable request.

Consent for publication

All authors have read and approved the final version of this manuscript. All authors consent to the publication of this work in its current form.

Contributors

SZ and HL designed and analyzed data, performed experiments, and wrote the manuscript. YS and YY contributed to the acquisition and interpretation of data. BY, CT and SL provided scientific input and revised the manuscript. YH, QK and XL supervised and conceived the entire project. YH is responsible for the overall content as the guarantor.

Ethics approval and consent to participate

This study was conducted in accordance with the Declaration of Helsinki and approved by the Ethics Committee of Harbin Medical University Cancer Hospital (Ethics Approval Number: KY2026-10). Written informed consent was obtained from all patients prior to tissue sample collection for the 80 TNBC cases included in the immunofluorescence analysis. All patient data were anonymized to protect privacy.

Funding Sources

This study was supported by grants from the WU JIEPING MEDICAL FOUNDATION (Grant No: 320.6750.2022-19-89), Beijing Medical Foundation (Grant No: MDK XUEYANZI 2023-1001) and Beijing Cancer Prevention &Treatment Society (Grant No: IZXUEYANZI 2023-1003).

References

1. Giaquinto AN, et al. Breast cancer statistics 2024. CA Cancer J Clin. 2024;74:477–95.
2. Waks AG, Winer EP. Breast cancer treatment: a review. JAMA. 2019;321:288–300.
3. Jiang Y-Z, et al. Molecular subtyping and genomic profiling expand precision medicine in refractory metastatic triple-negative breast cancer: the FUTURE trial. Cell Res. 2021;31:178–86.
4. Heeke AL, Tan AR. Checkpoint inhibitor therapy for metastatic triple-negative breast cancer. Cancer Metastasis Rev. 2021;40:537–47.
5. Li X, et al. Tumor-instructed glutamine synthesis in cancer-associated fibroblasts promotes pro-tumor macrophages. J Exp Med. 2025;222:e20241426.

6. Liu Y, et al. Tryptophan 2,3-dioxygenase-positive matrix fibroblasts fuel breast cancer lung metastasis via kynurenine-mediated ferroptosis resistance of metastatic cells and T cell dysfunction. Cancer Commun (lond Engl). 2024;44:1261–86.
7. Ben-Shmuel A, et al. Cancer-associated fibroblasts serve as decoys to suppress NK cell anticancer cytotoxicity in breast cancer. Cancer Discov. 2025;15:1247–69.
8. Sherman MH. CAFs defang NK cells to promote breast cancer immunosuppression. Cancer Discov. 2025;15:1096–8.
9. Ye F, et al. A novel peptide MIB1-223aa encoded by exosomal circMIB1 from cancer-associated fibroblasts drives triple-negative breast cancer metastasis and stemness via stabilizing MIB1 to activate notch signaling. J Adv Res. 2025;S2090–1232(25):433–3. 10.1016/j.jare.2025.06.023.
10. Fan G, et al. TSPAN8 + myofibroblastic cancer-associated fibroblasts promote chemoresistance in patients with breast cancer. Sci Transl Med. 2024;16:eadj5705.
11. Weigel C, et al. Sphingosine kinase 2 in stromal fibroblasts creates a hospitable tumor microenvironment in breast cancer. Cancer Res. 2023;83:553–67.
12. Xing Y, et al. RNA-binding protein BICC1 promotes gastric cancer progression via the PRRX1-MAPK signaling axis. Funct Integr Genomics. 2026;26:49.
13. Sun H, et al. BICC1 drives pancreatic cancer stemness and chemoresistance by facilitating tryptophan metabolism. Sci Adv. 2024;10:eadj8650.
14. Zhao R, et al. BICC1 as a novel prognostic biomarker in gastric cancer correlating with immune infiltrates. Int Immunopharmacol. 2020;87:106828.
15. Posta M, Győrffy B. Pathway-level mutational signatures predict breast cancer outcomes and reveal therapeutic targets. Br J Pharmacol. 2025;182:5734–47.
16. Wu SZ, et al. A single-cell and spatially resolved atlas of human breast cancers. Nat Genet. 2021;53:1334–47.
17. Andersson A et al. Spatial deconvolution of HER2-positive breast tumors reveals novel intercellular relationships. Preprint bioRxiv https://doi*org*/10.1101/2020.07.14.200600 (2020).
18. Bassiouni R, et al. Spatial transcriptomic analysis of a diverse patient cohort reveals a conserved architecture in triple-negative breast cancer. Cancer Res. 2023;83:34–48.
19. Dent R, et al. Triple-negative breast cancer: clinical features and patterns of recurrence. Clin Cancer Res : Off J Am Assoc Cancer Res. 2007;13:4429–34.
20. Sahai E, et al. A framework for advancing our understanding of cancer-associated fibroblasts. Nat Rev Cancer. 2020;20:174–86.
21. Parikainen M, Suwal U, Rappu P, Heino J, Sahlgren CM. Jagged1 regulates extracellular matrix deposition and remodeling in triple-negative breast cancer. Sci Adv. 2026;12:eaea9562.
22. Mao X, et al. Crosstalk between cancer-associated fibroblasts and immune cells in the tumor microenvironment: new findings and future perspectives. Mol Cancer. 2021;20:131.

23. Zhenkun, Liu, et al. AKAP12 positive fibroblast determines immunosuppressive contexture and immunotherapy response in patients with TNBC by promoting macrophage M2 polarization. J ImmunoTher Cancer. 2024;12:e009877.
24. Wang X, et al. AEBP1 drives fibroblast-mediated T cell dysfunction in tumors. Nat Commun. 2025;16:8171.
25. Öhlund D, et al. Distinct populations of inflammatory fibroblasts and myofibroblasts in pancreatic cancer. J Exp Med. 2017;214:579–96.
26. Liu R, et al. Emerging roles of angiopoietin-like 4 in human tumors (review). Int J Oncol. 2025;66:9.
27. Xiong Z, et al. Cancer-associated fibroblasts regulate mitochondrial metabolism and inhibit chemosensitivity via ANGPTL4-IQGAP1 axis in prostate cancer. J Adv Res. 2025;75:663–78.
28. Fan X, et al. FGF19-activated hepatic stellate cells release ANGPTL4 that promotes colorectal cancer liver metastasis. Adv Sci. 2025;12:e2413525.
29. Ohri N, et al. Gene expression dynamics in fibroblasts during early-stage murine pancreatic carcinogenesis. iScience. 2025;28:111572.
30. Zeng A, et al. Targeting OxLDL-mediated CD36 + CAF reprogramming potentiates PD-1 immunotherapy in osteosarcoma. Mol Cancer. 2025;25:14.
31. Li M, Zhou B, Zheng C. An integrated bioinformatic analysis of bulk and single-cell sequencing clarifies immune microenvironment and metabolic profiles of lung adenocarcinoma to predict immunotherapy efficacy. Front Cell Dev Biol. 2023;11:1163314.
32. Younis OM, et al. The role of ANGPTL4 in cancer: a meta-analysis of observational studies and multi-omics investigation. PLoS ONE. 2025;20:e0320343.
33. Habenicht L, et al. The role of the cell surface heparan sulfate proteoglycan syndecan-3 in breast cancer pathophysiology. Cells. 2025;14:1612.
34. Lee SY, et al. Syndecan-3 positively regulates the pro-inflammatory function of macrophages. Cell Mol LIFE Sci : CMLS. 2025;82:145.
35. Feng G, et al. Schwann cell-mediated M2-like macrophage polarization in rhabdomyosarcoma. Oral Dis. 2025;31:1140–53.

Figures

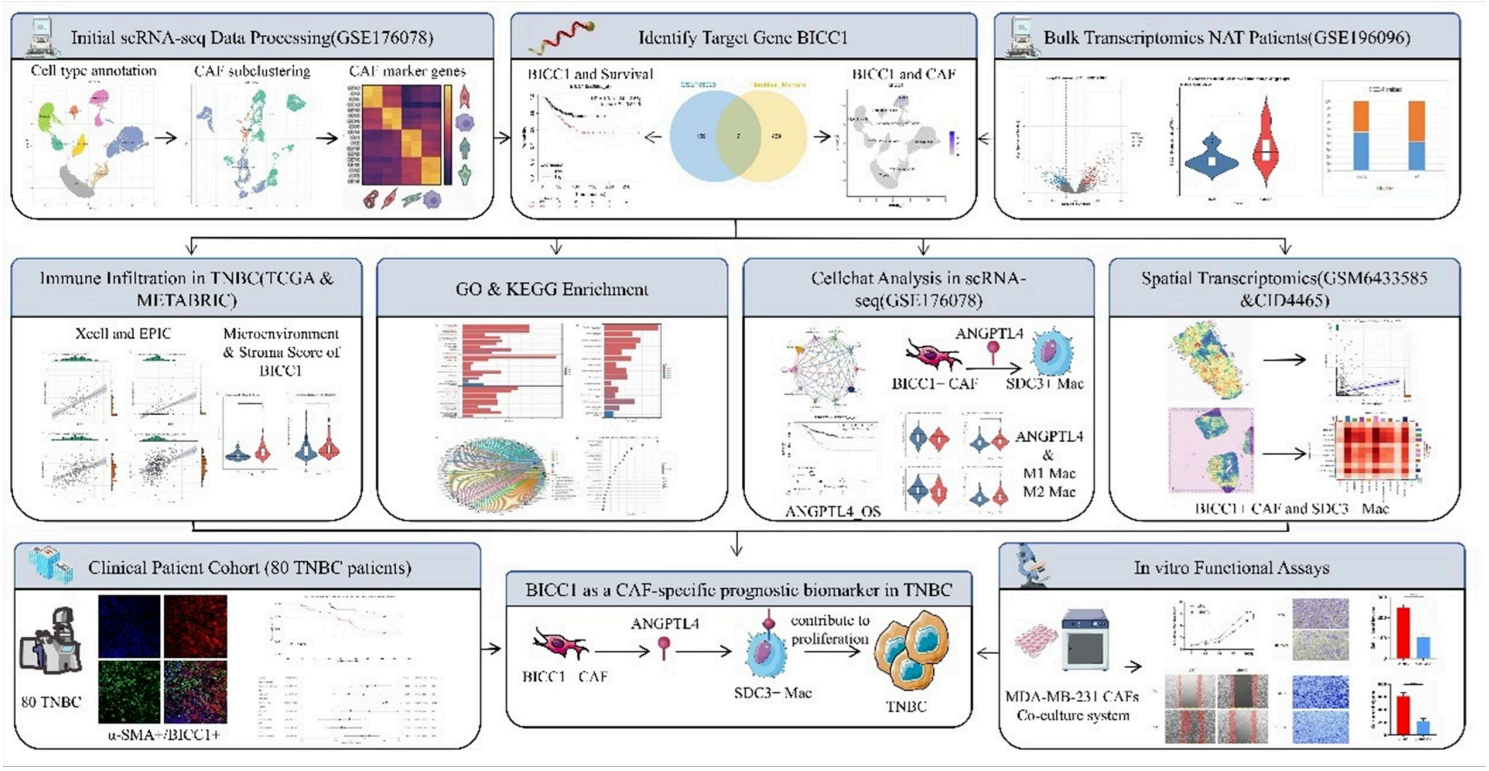


Figure 1

Flow Chart

CAF: Cancer associated fibroblast; NAT: neoadjuvant therapy; Mac: macrophage

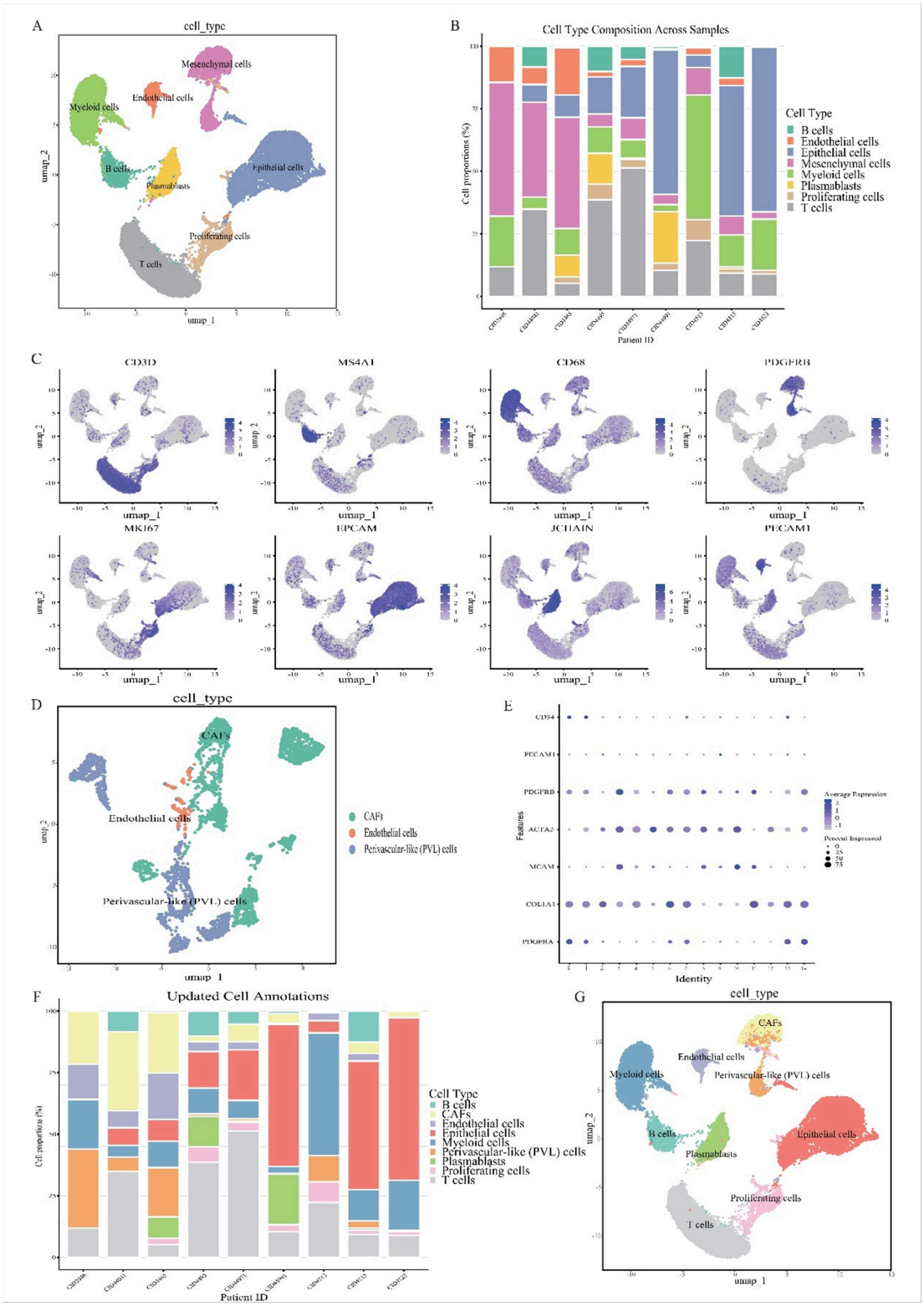


Figure 2

Annotation of fibroblast subtypes in TNBC. (A) The major cell types in the dataset were visualized using UMAP. (B)Cell type composition across patient samples. (C)Feature plots showing the expression of canonical marker genes across all cells: CD3D (T cells), MS4A1 (B cells), CD68 (myeloid cells), PDGFRB (mesenchymal cells), MKI67 (proliferating cells), EPCAM (epithelial cells), JCHAIN (plasmablasts), and PECAM1 (endothelial cells). Color intensity indicates normalized expression levels. (D)Subclustering of

mesenchymal cells revealing CAFs, endothelial cells, and perivascular-like (PVL) cells. (E)Marker gene expression patterns across mesenchymal subclusters. (F)Updated cell type composition after subcluster annotation. (G) UMAP visualization of all cell types following refined annotation.

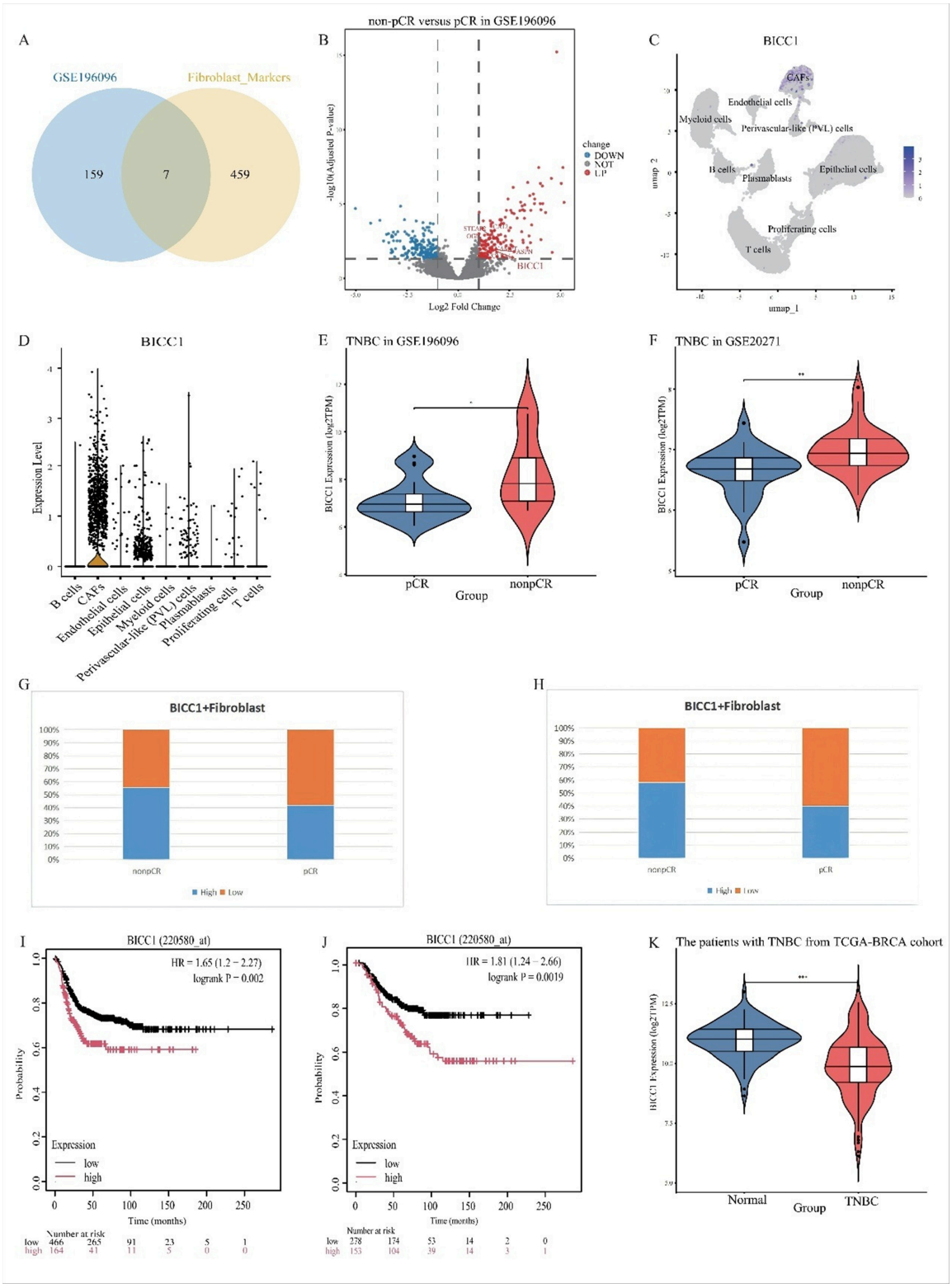


Figure 3

BICC1 is a CAF-associated gene associated with poor response and prognosis in TNBC. (A)Venn diagram showing the overlap between differentially expressed genes in non-pCR versus pCR patients (GSE196096) and fibroblast marker genes. (B)Volcano plot of differentially expressed genes between non-pCR and pCR groups in GSE196096 dataset. BICC1 is highlighted among significantly upregulated genes. (C)Feature plot showing BICC1 expression across single-cell clusters, with highest expression in CAFs. (D)Violin plot of BICC1 expression levels across different cell types. (E-F)BICC1 expression comparison between pCR and non-pCR groups in TNBC patients from GSE196096 and GSE20271. (G-H)Proportion of high and low BICC1+fibroblast signature in non-pCR versus pCR groups from GSE196096 and GSE20271. (I-J)Kaplan-Meier survival curves showing DMFS and OS based on BICC1 expression in TNBC patients. (K)BICC1 expression comparison between normal breast tissue and TNBC tumors from TCGA-BRCA cohort.

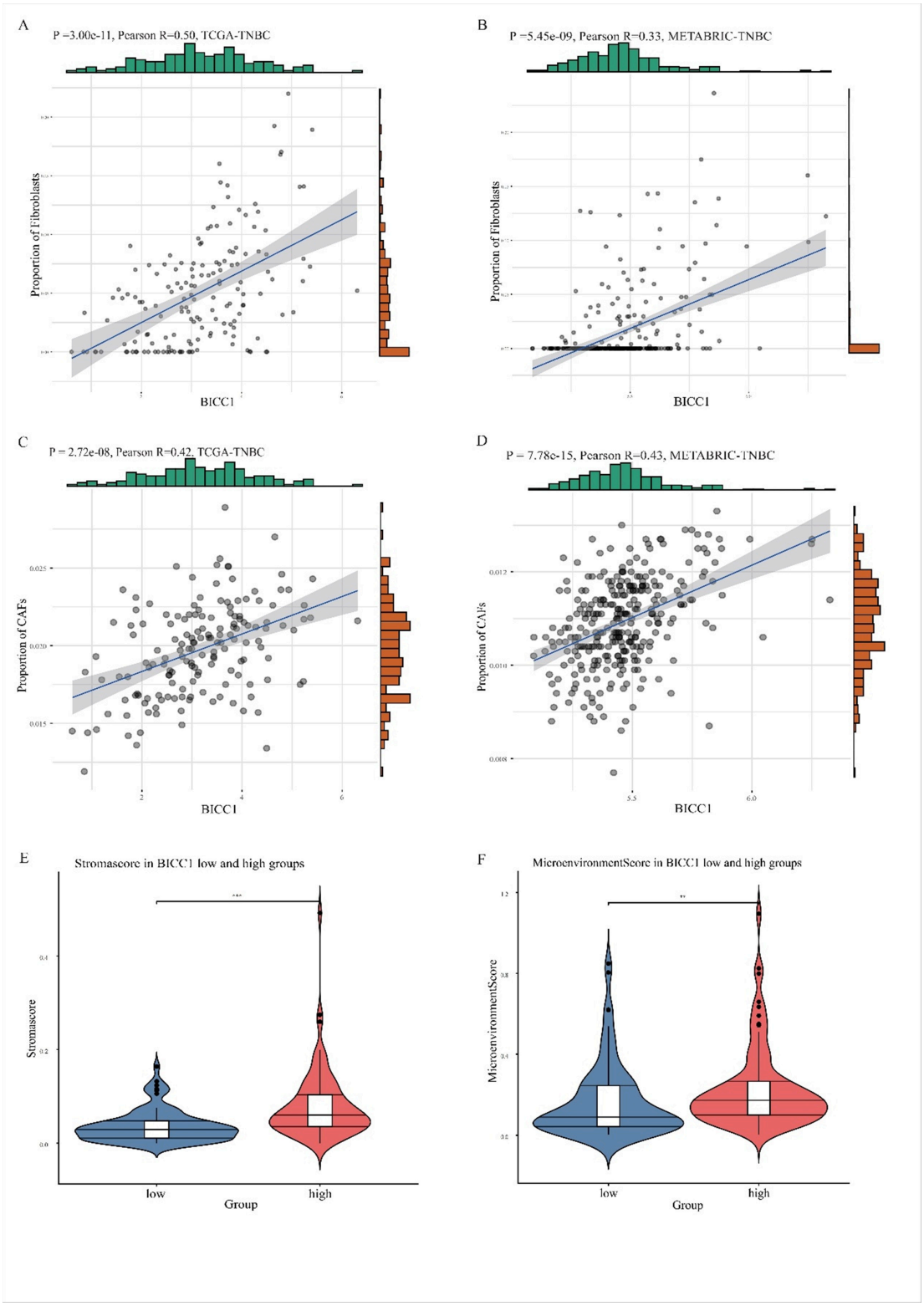


Figure 4

BICC1 correlates with fibroblast infiltration and tumor microenvironment in TNBC. (A)Correlation between BICC1 expression and fibroblast proportion in TCGA-TNBC through Xcell algorithm. (B)Correlation between BICC1 expression and fibroblast proportion in METABRIC-TNBC through Xcell algorithm. (C)Correlation between BICC1 expression and CAFs proportion in TCGA-TNBC through EPIC algorithm. (D)Correlation between BICC1 expression and CAFs proportion in METABRIC-TNBC through

EPIC algorithm. (E-F)Comparison of stromal score (E) and microenvironment score (F) between BICC1 low and high expression groups in TCGA-TNBC Xcell algorithm.

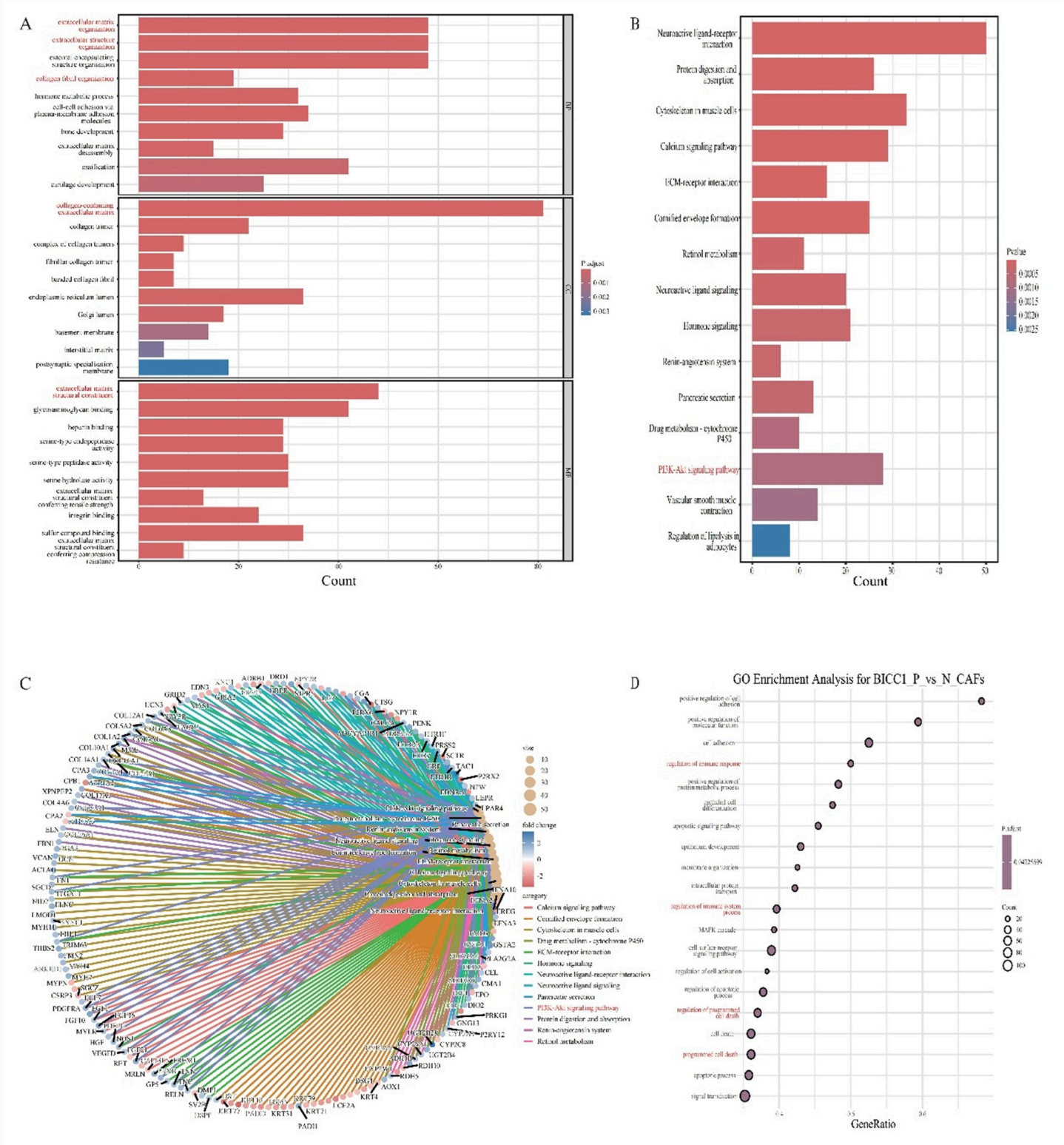


Figure 5

Functional enrichment analysis. (A)GO enrichment analysis. (B)KEGG pathway enrichment analysis. (C)A Circos plot depicting gene-pathway associations. (D)Dot plot of GO enrichment analysis for BICC1+

CAFs vs. BICC1-CAFs in TNBC.

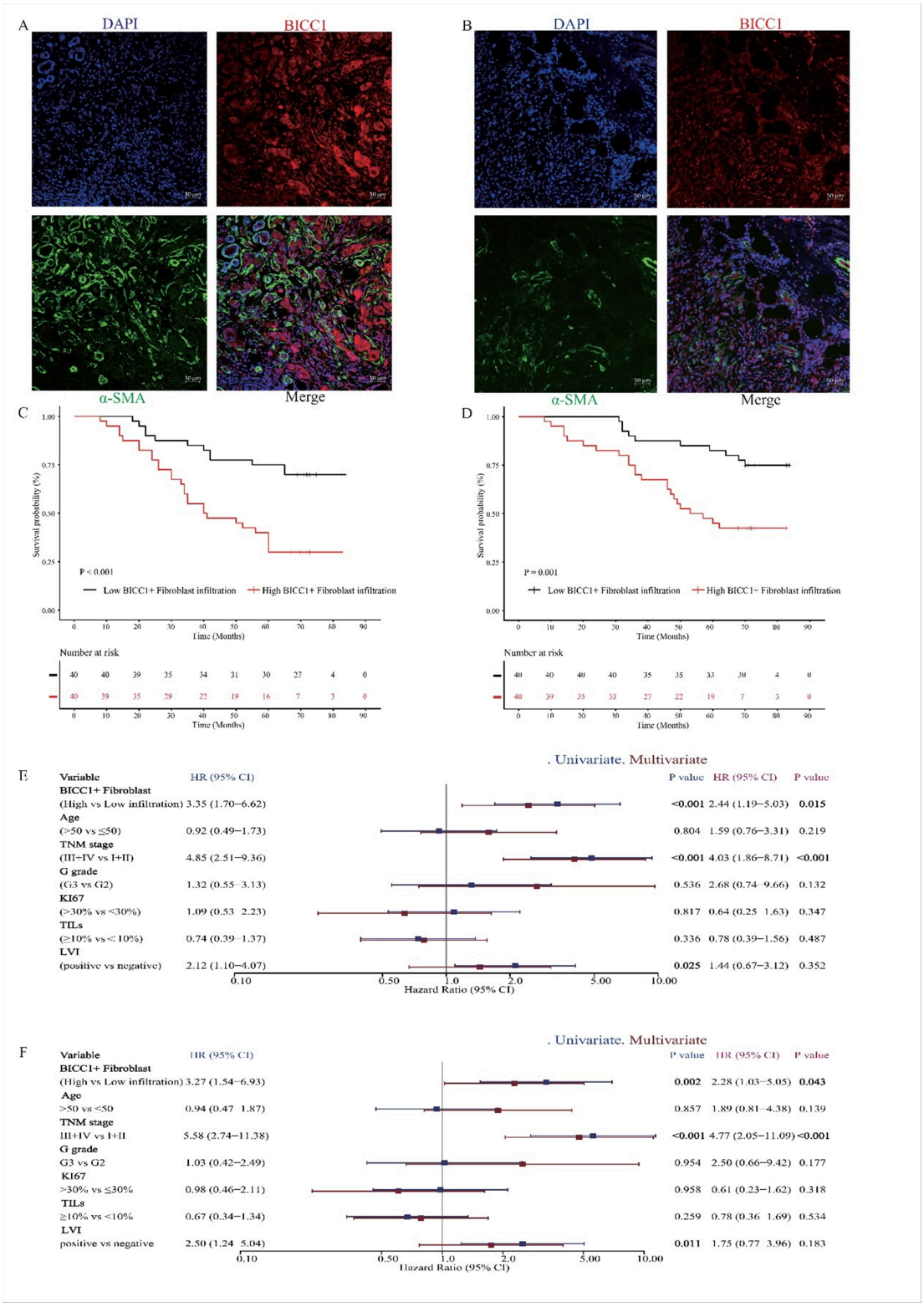


Figure 6

Prognostic value of BICC1+ CAFs in TNBC. (A-B)Immunofluorescence staining of BICC1 (red), α-SMA (green), and DAPI (blue) in tissues with high (A) and low (B) BICC1+ fibroblast infiltration. (C-D)Kaplan-Meier curves showing worse disease-free survival (C, P < 0.001) and overall survival (D, P = 0.001) in

patients with high BICC1+ fibroblast infiltration. (E-F) Univariate and multivariate Cox regression confirming BICC1+ fibroblast infiltration as an independent prognostic factor for both DFS(E) and OS(F). HR, hazard ratio; CI, confidence interval.

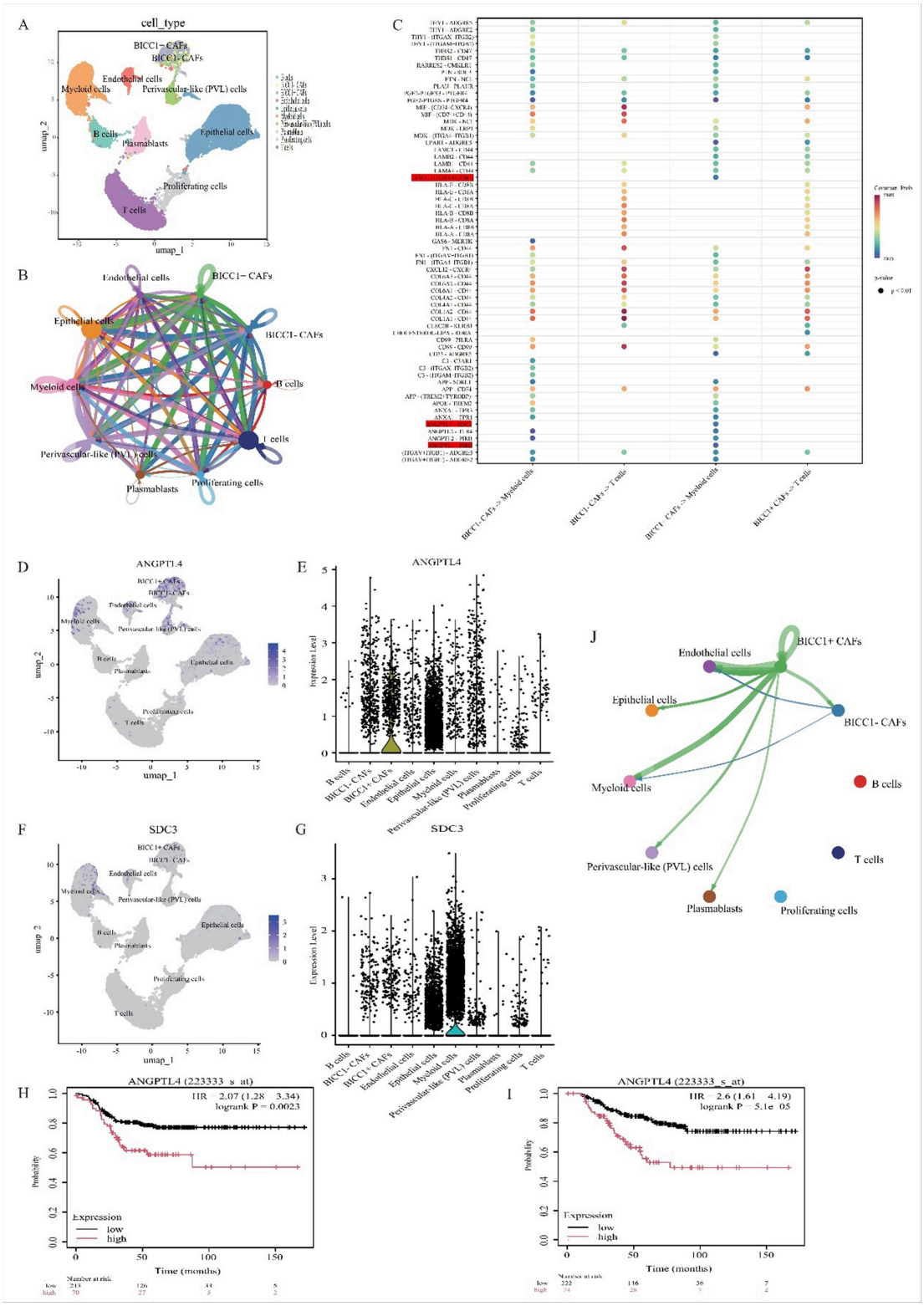


Figure 7

BICC1+ CAFs were characterized by specific signaling interactions and the expression of prognostic factors. (A) UMAP plot of major cell types. (B) Cell-cell communication network. (C) Top ligand-receptor pairs; color indicates communication probability, dot size indicates significance ($p < 0.01$). (D-F) UMAP feature plots showing ANGPTL4 (D) and SDC3 (F) expression. (E, G) Violin plots of ANGPTL4 (E) and SDC3 (G) expression across cell types. (H, I) Kaplan-Meier curves showing high ANGPTL4 expression correlates with poor survival (H:DMFS; I:OS). (J) Simplified network highlighting BICC1+ CAF interactions via the ANGPTL signaling pathway.

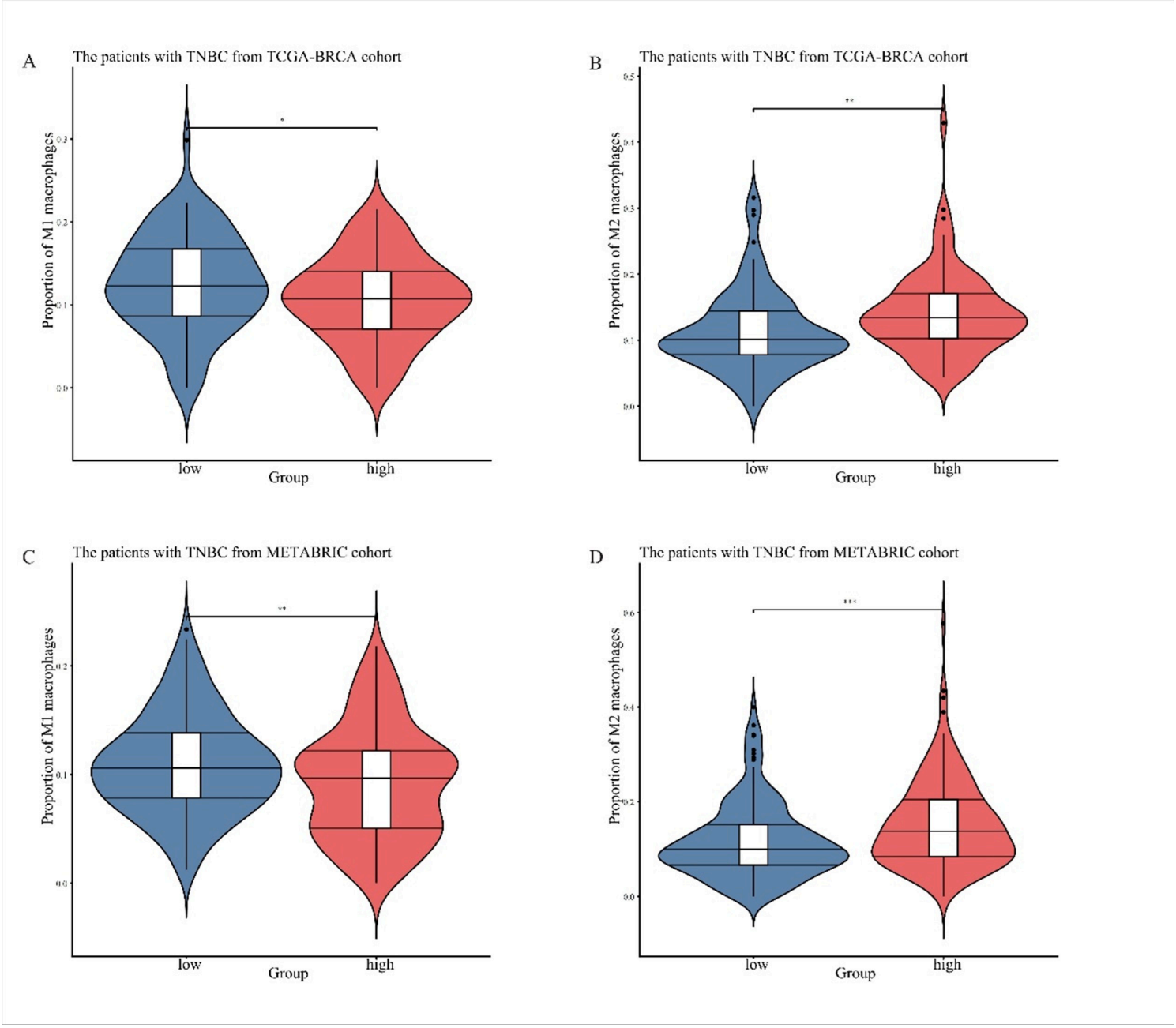


Figure 8

Association between ANGPTL4 expression and macrophage infiltration in TNBC through CIBERSORT. (A)Violin plots showing the proportions of M1 macrophages in TCGA-TNBC. (B) The proportions of M2

macrophages in TCGA-TNBC. (C) Violin plots showing the proportions of M1 macrophages in METABRIC-TNBC. (D) The proportions of M2 macrophages in METABRIC-TNBC.

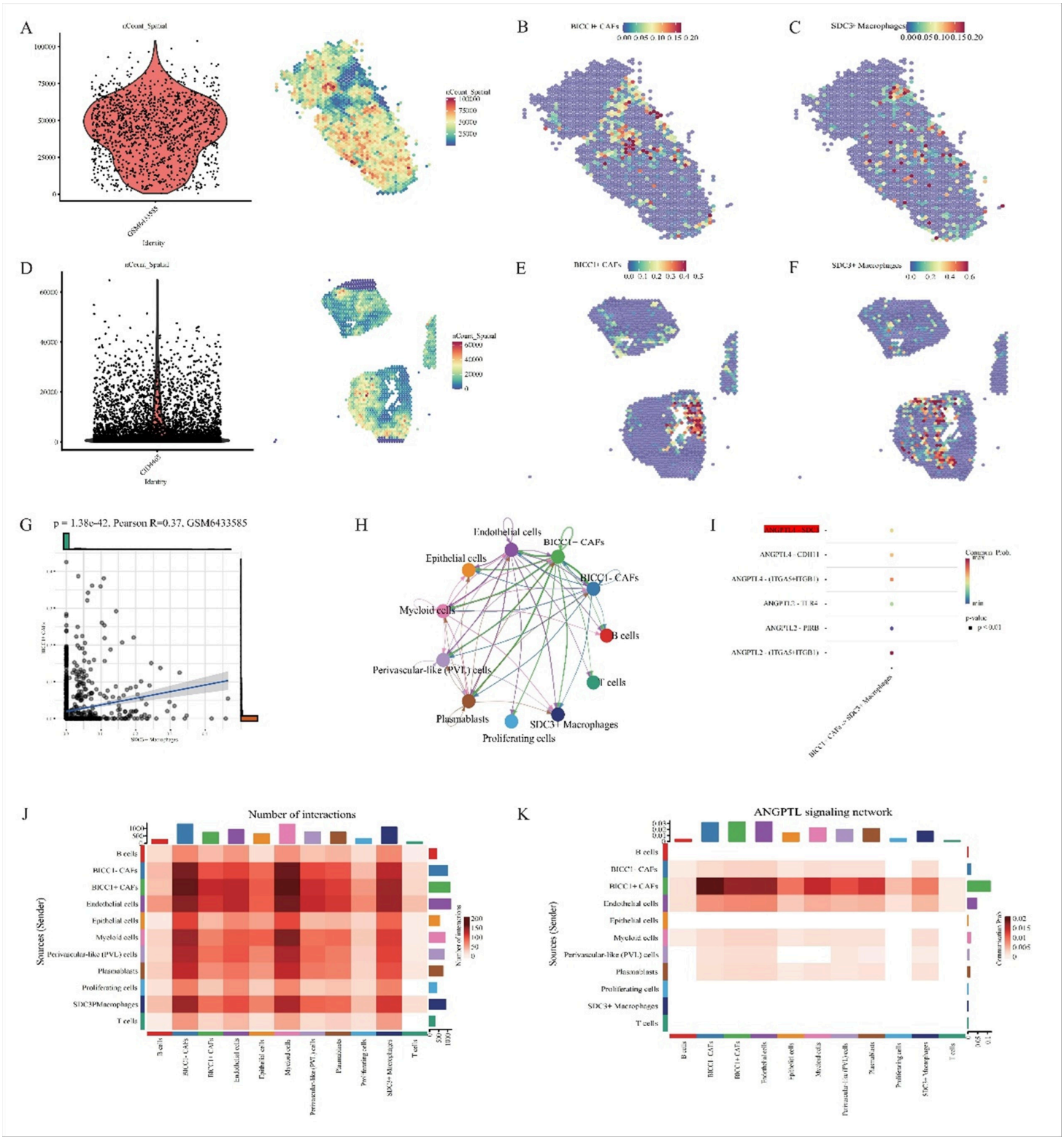


Figure 9

Spatial colocalization and ANGPTL-mediated communication between BICC1+ CAFs and SDC3+ macrophages. (A-D) Quality control and spatial distribution of UMI counts in samples GSM6433585 (A-

B) and CID4465 (C-D). (E-F) Spatial enrichment of BICC1+ CAFs (E) and SDC3+ macrophages (F) in sample CID4465. (G) Significant positive correlation between BICC1+ CAFs and SDC3+ macrophages abundance in GSM6433585. (H) Cell-cell interaction network among tumor microenvironment cell types. (I) Significant ligand-receptor pairs between BICC1+ CAFs and SDC3+ macrophages, highlighting ANGPTL4 and ANGPTL2 signaling axes. (J-K) Heatmaps showing total interaction numbers (J) and ANGPTL-specific communication probabilities (K) between cell type pairs.

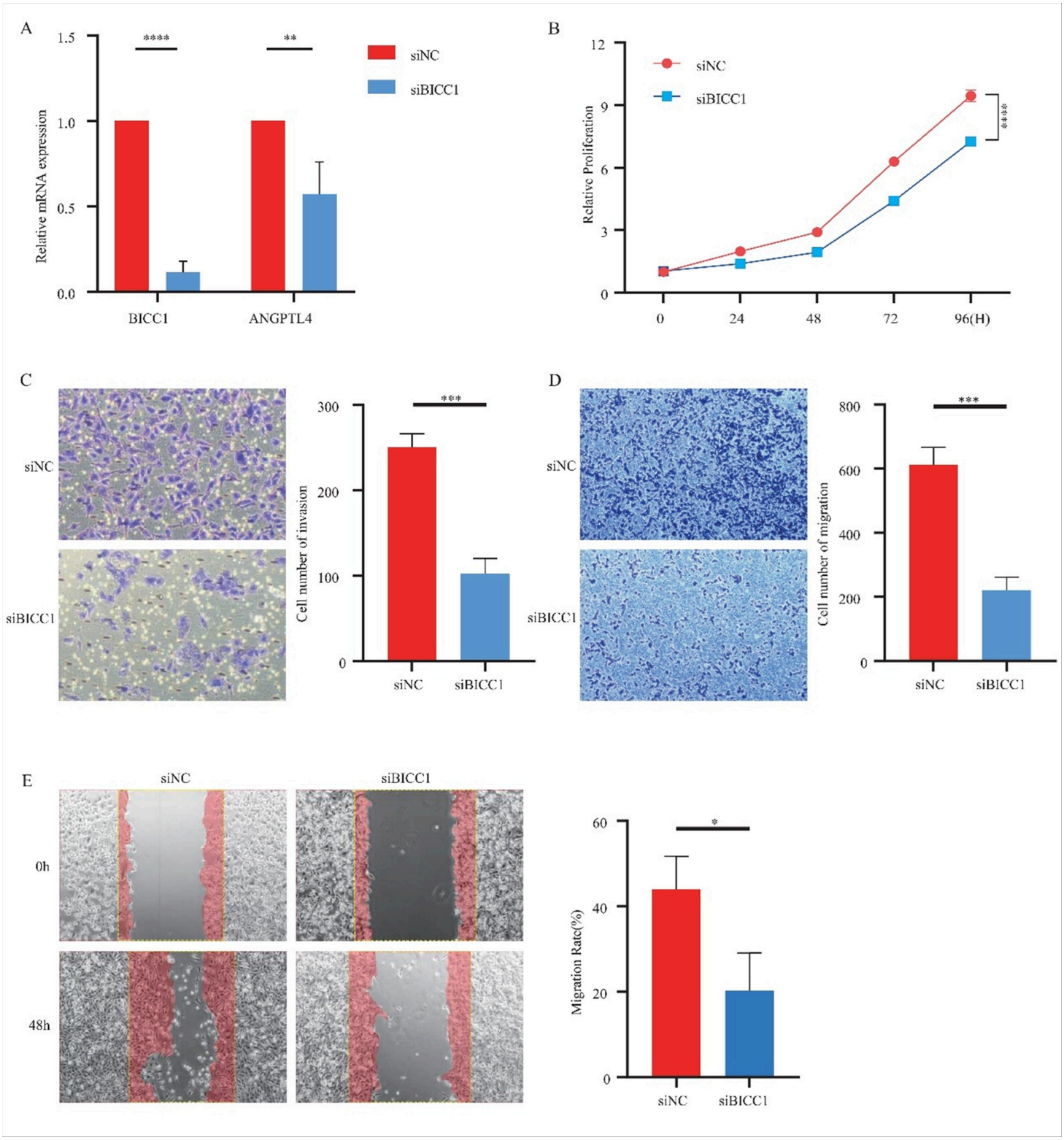


Figure 10

BICC1 knockdown suppresses TNBC cell proliferation, invasion, and migration. (A) qPCR analysis confirming knockdown efficiency of BICC1 and corresponding ANGPTL4 expression in MDA-MB-231 cells transfected with siBICC1 or control siRNA (siNC). (B) CCK-8 assay showing reduced proliferation of siBICC1-transfected cells over 96 hours. (C–D) Transwell assays evaluating invasion (C) and migration (D), indicating decreased invasive and migratory capacities after BICC1 knockdown. Representative images are shown on the left, with quantification on the right. (E) Wound healing assay demonstrating impaired migration of siBICC1 cells at 48 hours. Representative images (left) and migration rate quantification (right) are presented.

Supplementary Files

This is a list of supplementary files associated with this preprint. Click to download.

- FigS1.pdf
- FigS2.pdf